RSC Advances

PAPER

View Article Online
View Journal | View Issue

Cite this: *RSC Adv.*, 2025, **15**, 14643

Properties of 3D-printed continuous silk fiber-reinforced poly(caprolactone)

Zhengwei Yang,[abc] Linhui Huang,†[d] Xiaohui Song,*[bc] Minggan Wang,[e] Xingguo Han,[bc] Wenfang Guan[bc] and Chunlei Luo[bc]

Received 23rd February 2025
Accepted 6th April 2025

DOI: 10.1039/d5ra01302j

rsc.li/rsc-advances

In this study, poly(caprolactone)/continuous mulberry silk (PCL/MS) composite filaments were prepared *via* the pre-impregnation method and were employed for FDM technology. The MS was treated with alkali. The tensile properties and morphology of PCL/MS composite filaments were investigated using a universal mechanical testing machine and a scanning electron microscope. Results demonstrated that the incorporation of MS markedly enhanced the tensile properties of the filament. The interfacial adhesion between PCL and MS was dramatically improved after the NaOH treatment. The effects of print temperature on the flexural properties and porosity of the 3D-printed composites were examined. Results showed that a reduction in print temperature enhanced the flexural strength by 37.1%, and the porosity decreased from 35.33% to 15.29%. Finally, PCL/MS composite porous scaffolds with various pore sizes were fabricated successfully. These scaffolds exhibited excellent compressive strength and rigidity. The cell experiments showed that the composite scaffolds provided a non-toxic and favorable microenvironment for cells, supported both cell survival and proliferation, making them a promising candidate for further bone tissue engineering applications. Therefore, the results presented in this paper indicate that the PCL/MS composite scaffolds possessed the potential to serve as bone repair materials and facilitate their integration into human tissue engineering.

1. Introduction

Biodegradable polymers represent an optimal alternative to traditional polymers,[1] and possess high biocompatibility and excellent natural degradability.[2,3] In recent years, research and applications of biodegradable materials (such as PLA,[4] PGA,[5] PBS,[6] and PHB[7]) for medical purposes have been continuously developed.

Polycaprolactone (PCL) is a common biodegradable material with excellent drug permeability and good compatibility with organic polymers.[8] However, PCL exhibits inadequate hydrophilicity, poor cell adhesion, and inferior mechanical properties. The high crystallinity of PCL leads to a slow degradation rate, with the degradation occurring initially in the amorphous region. These shortcomings have restricted its medical applications.[9–12]

Compositing PCL with natural short fibers has gained extensive attention due to several advantages of natural fibers, including lightweight, renewability, degradability, non-toxicity, hydrophilicity and cost-effectiveness.[13–17] Karthi *et al.*[16] reviewed chemical treatments and applications of natural fiber-reinforced composites (sisal, jute, hemp *etc.*) and proved that natural fiber composites have wide advantages for the utilization of commercial and engineering applications. Sarasini *et al.*[18] prepared ramie fiber-reinforced PCL using low-temperature melt-molding, and found that the ramie fiber enhanced the tensile strength and modulus of PCL. Dhakal *et al.*[19] used a twin-screw extruder to prepare hemp fiber/PCL bio-composites and investigated the nano-mechanical and the thermal properties. Moreover, Rafał *et al.*[20] observed that the PCL/hemp composite exhibited a higher flexural modulus when the hemp content was over 10 wt%. However, this increase in flexural modulus was accompanied by a decrease in elongation at break and impact strength. This phenomenon can be attributed to the excessive proportion of natural short fibers and their uneven distribution in polymer matrix. Therefore, the overall improvement of the composite's mechanical properties was restricted by the ratio of natural fiber in composites. Moreover, these studies adopted traditional methods to prepare

[a]*School of Materials Science and Engineering, Guilin University of Electronic Technology, Guilin 541000, China*

[b]*Key Laboratory of Special Engineering Equipment Design and Intelligent Driving Technology (Guilin University of Aerospace Technology), Education Department of Guangxi Zhuang Autonomous Region, China. E-mail: songxiaohui2010@163.com*

[c]*Guangxi Key Laboratory of Special Engineering Equipment and Control, Guilin University of Aerospace Technology, Guilin 541004, China*

[d]*Guangxi Key Laboratory of Oral and Maxillofacial Rehabilitation and Reconstruction, College & Hospital of Stomatology, Guangxi Medical University, Nanning, 530021, China*

[e]*School of Mechanical and Control Engineering, Guilin University of Technology, Guilin 541000, China*

† These authors contributed to the work equally and should be regarded as co-first authors.

PCL/natural fiber composites, which may not meet the requirements of bone scaffolds used in TE.

Natural continuous fibers exhibited higher mechanical strength than short fibers and are much cheaper than unnatural fibers, for example continuous carbon fiber and glass fiber. Silk, derived from silkworm, has been applied in tissue engineering,[21] drug delivery systems,[22] dressings[23] due to its favorable mechanical properties, biocompatibility and controllable biodegradability.[24–26] To prepare porous scaffolds with continuous silk fiber, researchers have done considerable work. Zhang *et al.*[27] obtained electrospun PCL/silk film, and found that spider silk fibroin enhanced the hydrophilicity, cell proliferation and adhesion of PCL. Li[28] prepared silk fiber/PCL composites by using hot-pressing and found that the composites exhibited a positive correlation between mechanical strength and the proportion of silk. Shi *et al.*[29] applied *Bombyx mori* (Bm) silk, and *Antheraea pernyi* (Ap) silk to prepare filament composite with PCL using melt extrusion. They concluded that the effect of Ap addition was more pronounced than that of Bm. As the volume content of Ap increased from 15% to 20%, the tensile strength of the PCL composites improved from 82.8 to 105.9 MPa. However, the author did not study other mechanical properties.

Additive manufacturing (AM), also known as 3D printing, can directly fabricate a part with complex inner and outer structure from digital 3D model,[30,31] and is very suitable to the porous structure of bone scaffolds. FDM is one of the widely used AM technologies due to its high flexibility and low cost.[32,33] Nowadays, FDM have been employed to deal with PCL/polysaccharide,[34] PCL/TPU,[35] PCL/PLA composites[36] and so on. Meanwhile, the FDM of continuous fiber-reinforced composites, such as continuous carbon fiber (CF)/PCL[37] and continuous glass fiber (GF)/PCL,[38] has also been widely applied. However, only few studies were related to FDM of PCL/natural continuous fiber composites. Hedayati *et al.*[5] used continuous polyglycolic acid (PGA) to reinforce PCL, and printed PGA/PCL composite scaffold by FDM. However, the FDM process for continuous mulberry silk fiber reinforced PCL composites has not yet been studied.

Therefore, this study fabricated natural continuous mulberry silk fiber/PCL (MS/PCL) composites with FDM. The main contents included surface treatment of MS; pre-impregnating MS with PCL melts *via* a lab-made single screw extruder; investigating the effect of fiber volume contents on the tensile properties of the MS/PCL composite filament; exploring the impact of print temperature on the flexural properties of 3D printed MS/PCL composites; and evaluating the performance of MS/PCL composite scaffolds.

2. Experimental methodology

2.1. Materials

Polycaprolactone 6500, a medical-grade polymer produced by Perstorp, Sweden, was purchased from a Taobao supplier in powder form. The characteristics provided by the supplier include an average molecular weight of 80 000 g mol^{-1}, a water content of 0.35%, a melting point of 59 °C, a melt flow index of 3 g/10 min (160 °C, 5 kg). Mulberry silk (MS) 630 D with diameter about 1.5 mm, was obtained from Shanxi, China. As shown in Fig. 1.

Fig. 1 Picture of natural mulberry silk cord.

The surface of MS was treated with an alkaline solution to improve hydrophilicity and enhance interfacial compatibility with the polymer matrix.[39] The MS was soaked in a 5 wt% NaOH solution for 10, 15, 20 and 25 min, respectively; then, the MS was washed with deionized water to remove residual NaOH; finally, the treated MS was dried in a hot-air oven at 45 °C for 4 h.[40–45]

2.2. Composites preparation

A lab-made single-screw extruder was employed to impregnate MS with the PCL melt. Through trial and error, the optimal extrusion parameters were identified (Table 1) as the mould temperature of 80 °C, a barrel temperature of 85 °C, and a screw speed of 15 rpm. The diameter of the composite filaments and the MS content in the composite filaments was designed to be in the range of 1.4–1.9 mm and 23.68–31.03%, respectively, by varying the diameter of extruder die.

Pure PCL, PCL/MS NaOH-treated filaments (PMN), and PCL/MS-untreated filaments (PMU, diameter in 1.43, 1.67 and 1.9 mm) were prepared with various screw speeds (10, 15 and 20 rpm), as illustrated in Fig. 2.

PCL/MS composite filaments were fed into the FDM machine (Allct 334, China). The processing parameters were as follows: a printing speed (V) of 15 mm s^{-1}, a layer thickness (H) of 0.8 mm, a nozzle diameter of 1.0 mm, and a platform temperature of 20 °C. Various print temperatures were set (90 °C, 100 °C, 110 °C and 120 °C). The G-code created automatically with slicing software was not able to meet the requirements for the continuity of MS. Therefore, the G-code was re-edited to 3D print the PCL/MS composite filaments continuously without any cut-off. The printing path of the fleruxal specimen is illustrated in Fig. 3a, where the printing nozzle completes one layer by moving sequentially from the starting points A to B, C, and D. Each flexural specimen was fabricated with four layers, and each layer contained six printed rows. The square porous specimens were fabricated by alternating the printing directions (0° and 90°) between successive layers, following

Table 1 Extrusion parameters for PCL/MS composite filaments

Specimen	NaOH modified	Screw speed (rpm)	Diameter (mm)	Fiber volume fraction (%)
D0	No	15	1.70	0
D1	No	20	1.45	31.03
D2	No	15	1.70	26.47
D3	No	10	1.90	23.68
D2N10	Yes	15	1.70	26.47
D2N15	Yes	15	1.70	26.47
D2N20	Yes	15	1.70	26.47
D2N25	Yes	15	1.70	26.47

a repetitive path from the starting point E to F' (F) and then to E' (Fig. 3b). Each porous specimen was constructed with five layers, with pore size regulation achieved by precisely adjusting the printing linewidth.

In accordance with the ISO 14125 standard, specimens with dimensions of 80 mm × 10 mm × 4 mm were prepared to investigate the effect of print temperature on flexural properties. Based on the standard GB/T 1041, square porous compression specimens with dimension of 30 mm × 30 mm × 5 mm were prepared. The designed porous specimens were fabricated with pores of 2, 2.5, and 3 mm.

2.3. Materials characterization

Based on the standard GB/T 228.1-2010, the tensile properties of the pre-impregnated filaments were characterized using an electronic universal testing machine (UTM5105, Shenzhen, China), with a testing rate of 2 mm min^{-1} and a preload of 0.1 N. Each group of specimens yielded provided three sets of valid data, which were then averaged to obtain the final test value. To hold the filaments and avoid slipping during the tensile test, a special fixture (in white color) was developed, as shown in Fig. 4.

In accordance with the ISO 14125 standard, the three-point flexural test for 3D-printed PCL/MS composites was conducted using an electronic universal testing machine (UTM5105, Shenzhen, China). The test speed was set to 0.5 mm min^{-1}.

According to the standard GB/T 1041-2008, the compressive properties of the 3D-printed porous scaffolds were evaluated using the same electronic universal testing machine (UTM5105, Shenzhen, China) with a compression rate of 1 mm min^{-1}.

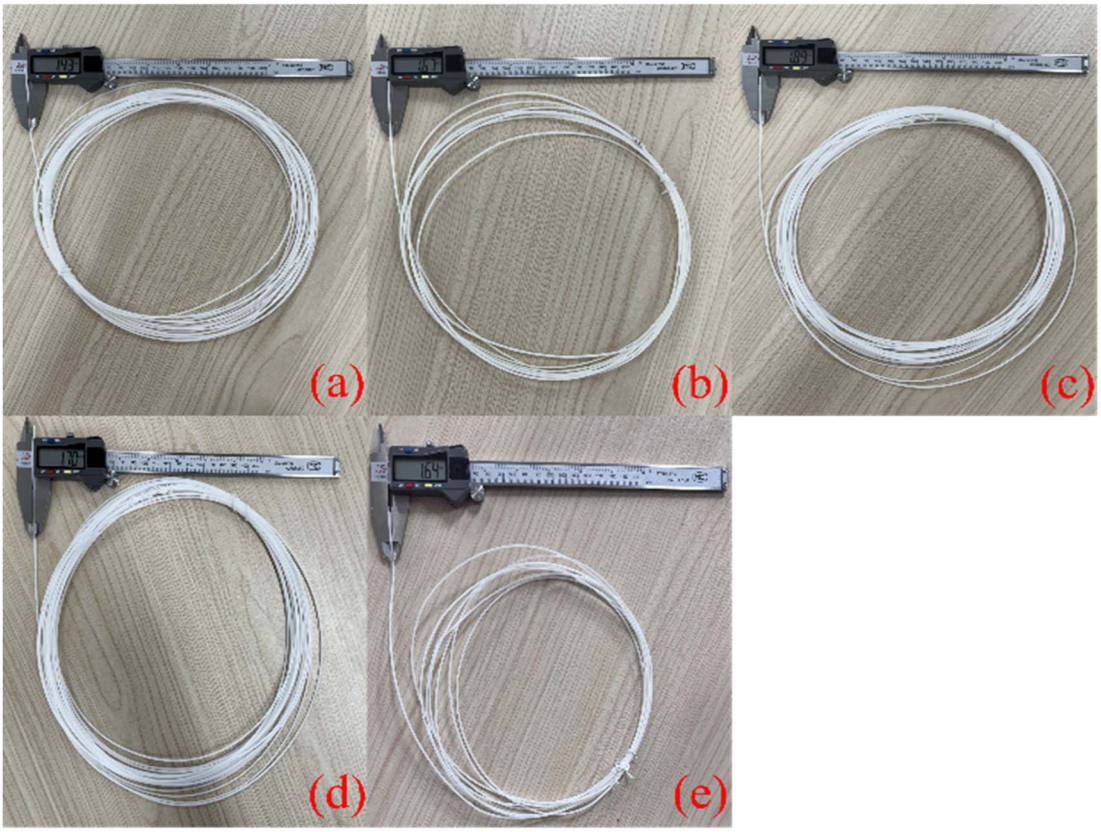

Fig. 2 Pictures of the prepared composite filaments: (a) PMU-D1, (b) PMU-D2, (c) PMU-D3, (d) PMN-D2, and (e) pure PCL-D0.

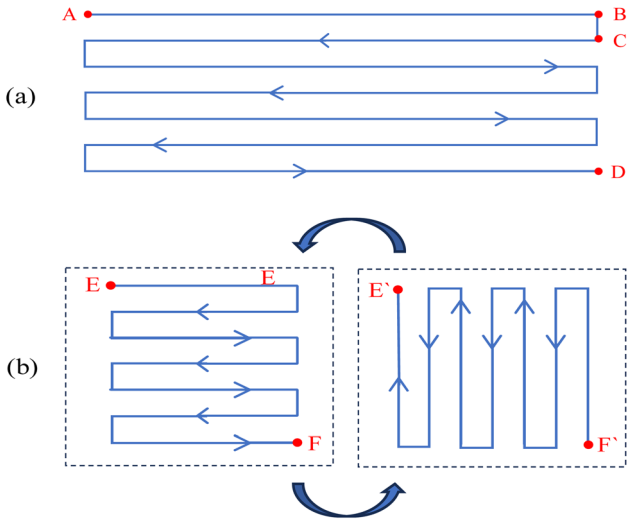

Fig. 3 Path planning of specimens: (a) flexural specimens and (b) square porous scaffolds.

Fig. 4 Tensile tests of PCL/MS filaments while under load.

The porosity of the flexural specimen composites can be calculated using the following eqn (1):

$$P = 100 - \rho_m(w_r/\rho_r + w_s/\rho_s), \quad (1)$$

where P is the porosity of the specimen being calculated, ρ_m is the apparent density of the composite (g cm^{-3}), determined by the drainage method, ρ_r and ρ_s are the densities of MS and PCL, which are 1.14 g cm^{-3} and 1.25 g cm^{-3}, respectively, as provided by the supplier. w_r and w_s are the mass fractions of PCL and MS, respectively. The average density of the three specimens in each group was taken as the apparent density of the PCL/MS composite.

The tensile fracture surface of the filaments and the square porous microstructure of the scaffolds were examined using scanning electron microscopy (SEM, VEGA 3 SBH, Czech). Given the non-conductivity of PCL, all specimens were coated with gold prior to scanning.

The PCL/MS composite filaments were characterized using fourier transform infrared spectroscopy (FTIR, FTIR-650, China). A single attenuated total reflection (ATR) method was employed, with a small piece of the composite filament pressed against a ZnSe crystal using a pressure rod. The infrared spectrum ranged from 4000 to 500 cm^{-1}, with a spectral resolution of 4 cm^{-1}.

MC3T3-E1 mouse embryonic osteoblast precursor cells (Shanghai Yu Bo Biotech Co., Ltd) were cultured in α-MEM basic medium (Gibco, U.K.) supplemented with 10% (w/v) fetal bovine serum (FBS; OriCell New Zealand) and 1% (10 000 U mL^{-1}) penicillin/streptomycin (Solarbio, China). Cultures were maintained at 37 °C in a humidified atmosphere containing 5% CO_2, with medium changes every two days.

The CCK-8 kit (UElandy3, China) was used to evaluate the cytotoxicity of the cells on the scaffolds. MC3T3-E1 cells were separately seeded on the surface of different scaffolds in 48-well plates and then incubated for 72 hours. At 72 hour time point, 500 μL of cell culture medium containing 10% CCK-8 solution was added to each well and incubated for 1 hour at 37 °C. Subsequently, 100 μL of the medium from each well was transferred into a new 96-well plate, the optical density (OD) at 450 nm was detected using a microplate reader (Tecan Infinite® 200 PRO, Austria). Cell viability (%) was calculated using the formula:

$$\text{Cell viability (\%)} = (A_e - A_n)/(A_p - A_n) \times 100\%,$$

where A_p is the absorbance of the positive control group, A_n is the absorbance of the negative control group, and A_e is the absorbance of the experimental group.

Live/dead staining was conducted to assess cell survival on the scaffolds. MC3T3-E1 cells were seeded onto the scaffolds in 48-well plates and incubated for 72 h. The samples were then rinsed with PBS for 3 times and incubated with Calcein-AM/PI solution (Bigtime, China) for 15 min. Fluorescent images were captured using an inverted fluorescence microscope (EVOS FL Auto2, Thermo Scientific, USA) (Fig. 5).

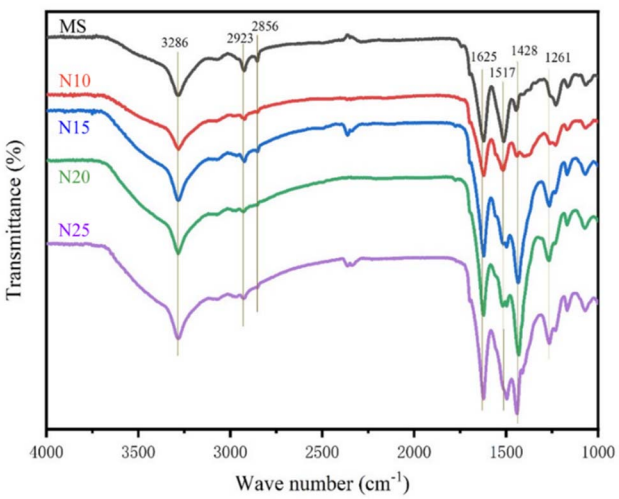

Fig. 5 FTIR of untreated and NaOH-treated MS filaments.

3. Results and discussion

3.1. FTIR analysis of untreated and NaOH-treated filament

The FTIR spectra of MS are presented in Fig. 5, illustrating the impact of NaOH modification time on the functional groups of the silk. The presence of hydrogen-bonded O–H groups was evidenced by a distinct O–H stretching vibration peak at 3286 cm^{-1},[40] which was gradually weaker with the increase of NaOH treatment time (N10, N15, N20, N25). This observation suggested the breakage of hydrogen bonds, and the hydroxyl groups in the silk may have been partially degraded or reacted with other molecules following NaOH treatment.[41] The bands at 2923 cm^{-1} and 2856 cm^{-1}, corresponding to the C–H stretching vibrations of CH_2 or CH_3 groups in silk, also exhibited varying degrees of attenuation with longer NaOH treatment times. This indicated that NaOH has exerted a certain effect on the aliphatic hydrocarbon chains within the silk.[42] 1625 cm^{-1} and 1517 cm^{-1} bands represented the amide I band (C=O stretching vibration) and amide II band (N–H bending vibration) in the molecular structure of silk proteins,[43] respectively. The marked changes in the intensity of these vibration peaks with increasing NaOH treatment time suggested that the NaOH treatment has broken some of the amide bonds, allowing partial denaturation or hydrolysis of the protein structure in the silk.[44] Band 1428 cm^{-1} was related to CH_2 shear vibrations. With the prolongation of NaOH treatment, partial hydrolysis of the amorphous regions in the silk occurred, leading to the rearrangement and increase of its side chains.[45] The change at 1261 cm^{-1} was mainly associated with the amide III band (C–N stretching vibration and N–H bending vibration) NaOH treatment caused a shift from a random coil structure to a more ordered β-folded structure in the silk, and the proportion of the β-folded structure increased with the prolongation of NaOH treatment, leading to an enhancement of the intensity of this absorption peak.[45]

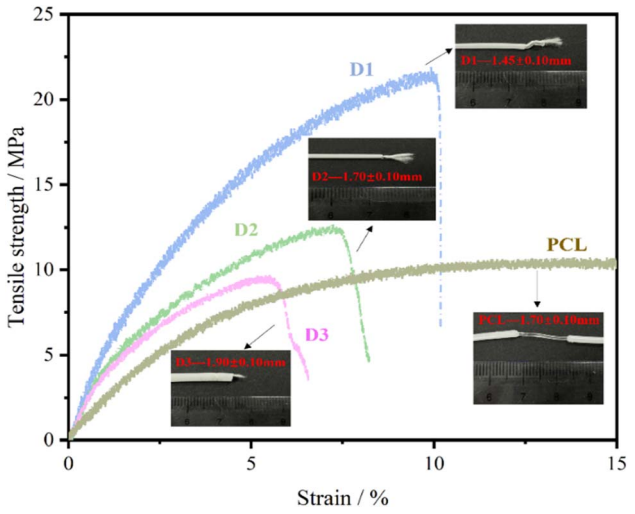

Fig. 6 Effect of MS-untreated content on the tensile properties of PMU composite filaments.

3.2. Tensile properties of filament affected by the volume content of MS

Fig. 6 and Table 2 display the tensile properties of pure PCL and PMU composite filaments. The tensile properties were positively related to the weight content of MS in the composite filaments (23.68–31.03%), but negatively related to the diameter of PMU filament (1.45–1.9 mm). The maximum values were 21.02 MPa and 9.96% at D1. The crystalline structure and orderly molecular chain arrangement of MS endows it with high tensile strength (360 MPa),[46,47] effectively compensating for the tensile deficiencies of the PCL matrix.

In Fig. 6, the filament of pure PCL after being stretched exhibited a long necking and a maximum tensile strain (over 15%), indicating good toughness. The incorporation of untreated MS reduced the toughness of PCL. When the content of untreated MS was 23.68%, MS and PCL fractured at the same time with a shorter MS fiber being stretched out from PCL. Fortunately, with increasing MS content, the situation of toughness was gradually improved. From the filament picture of D1, it can be seen that the PCL and MS were stretched together initially before breaking, indicating improved interfacial compatibility. Therefore, PCL and MS created a complementary system with enhanced overall performance,[48] where the former contributed to toughness, and the MS contributed to strength.

Similar studies have demonstrated comparable results. Shi *et al.*[49] demonstrated that the tensile property of silk/PCL composite filament can be improved when the content of silk was more than 10%. When the volumetric fraction of silk was 20 vol%, the silk/PCL composite filament had the highest tensile modulus and strength (1.95 GPa, 105.9 MPa). The incorporation of silk enhanced the tensile strength of PVA/silk composite from 15.9 to 45.87 MPa, but significantly declined the tensile strain dramatically from 140% to about 15%.[50] The silk in these two studies was not treated with any physical or chemical methods, resulting in the reduction of tensile strain. Therefore, in the following study, alkali treatment was employed to improve the comprehensive tensile properties of PCL/MS filaments.

Table 2 Tensile properties of PMU composite filaments

Specimen	Diameter (mm)	Tensile strength (MPa)	Tensile strain (%)	Fiber volume content (%)
D0	1.70 ± 0.10	10.21 ± 1.02	15.00	—
D1	1.45 ± 0.10	21.02 ± 2.19	9.96 ± 0.59	31.03 ± 0.76
D2	1.70 ± 0.10	12.57 ± 1.46	7.40 ± 0.71	26.47 ± 0.98
D3	1.95 ± 0.10	9.52 ± 1.50	5.51 ± 0.85	23.68 ± 0.84

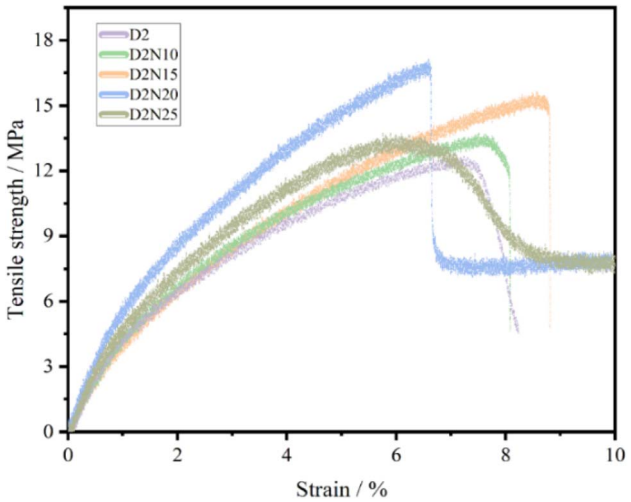

Fig. 7 Stress–strain curves of tensile properties of PCL/MS composite filaments affected by NaOH treatment time.

3.3. Tensile properties of filaments affected by the treatment time of MS

Fig. 7 and Table 3 show the influence of the different NaOH treatment times on the tensile properties of PCL/MS composite filaments with the same MS volume content (26.47%), D2N10, D2N15, D2N20 and D2N25 represent the specimens with alkali treatment times of 10, 15, 20 and 25 min, respectively. The curves of D2, D2N10 and D2N15 showed one stage of elastic deformation and broke at the yield point, indicating a brittle break. The tensile strength and strain of these samples increased gradually from 12.57 MPa and 7.4% to 15.54 MPa and 8.76% with the extension of treatment time from 0 to 15 min. When the treatment time was extended to 20 min, the curve of D2N20 exhibited two steps of break, the first one was the break of silk, and the second corresponded to the break of PCL, indicating an enhancement of interfacial compatibility between PCL and MS. The curve of D2N25 demonstrated two stages, elastic and yield deformation, and remained unbroken until the strain of 10%, indicating an excellent interfacial compatibility between PCL and MS. A study also demonstrated that natural fibers can be modified by alkali treatment, thereby improving the various properties of bio-composites.[51]

The improvement of tensile properties can be explained as follows: the FTIR results have proved that NaOH treatment disrupted the hydroxyl groups and hydrolyzed the protein structure of silk, resulting in a loosened microstructure. Meanwhile, the alkali solution has a strong etching effect on silk, leading to a rough surface. Therefore, the loosen microstructure and rough surface enlarged the contact area of silk with PCL, promoted mechanical interlocking and thereby strengthened the physical bonding,[52] and finally improved the tensile strength and strain.

Fig. 8 shows the comparison of tensile fracture morphology of PCL/MS composite filaments before and after NaOH treatment at various times. The fracture surface of the MS without being treated with NaOH (Fig. 8a) exhibited a relatively flat fracture, and the MS fibers had not undergone any significant elongation, and there was a considerable gap between the MS and matrix (Fig. 8a1, green rectangle), indicating a lack of compatibility and inadequate impregnation. Under the treatment of alkali, the fracture surface of the NaOH-treated filaments began to show significant cracks (Fig. 8b, blue arrow). These cracks served to dissipate tensile energy, thereby enhancing the tensile strength of the filament. The fiber tow ruptured and spread apart, reducing the gap between the fiber and the matrix, resulting in a stronger bond between them. It can be seen that the MS fiber adjacent to the PCL matrix was embedded in the PCL. (Fig. 8b1, blue rectangle) This result indicated that the treatment of NaOH improved the interfacial compatibility. The interfacial bonding strength between MS and PCL gradually increased with the prolongation of alkali treatment time. At D2N20 (Fig. 8d), the MS were uniformly distributed in the PCL matrix and less fiber withdrawal occurred (Fig. 8d1, purple rectangle). When the composite filament was subjected to tensile loading, the crack extension to the vicinity of the MS was deflected or bifurcated, which increased the crack extension path (purple arrow).

This crack steering effect effectively slowed down the crack expansion and improved the fracture toughness of the material; in addition, the silk fibers in the PCL matrix formed an effective "pinning" effect, thus hindering the rapid expansion of the cracks, and increasing the energy dissipation in the process of silk material tensile fracture. However, when the alkali treatment time was too short (D2N10 Fig. 8b and D2N15 Fig. 8c), the MS were more likely to be withdrawn during the stretching process. The crack steering effect was not significant, indicating a weak interfacial bond. An excessively long alkali treatment time (D2N25 Fig. 8e), although promoting interfacial bonding between MS and PCL, caused more PCL cover the silk (Fig. 8e1, white rectangle), which may lead to fiber embrittlement and ineffective steering of the crack path, resulting in a decrease in tensile property.

Table 3 Tensile properties of PMN composite filaments

Specimen	NaOH treatment time (min)	Diameter (mm)	Tensile strength (MPa)	Tensile strain (%)
D2	0	1.70 ± 0.10	12.57 ± 1.46	7.40 ± 0.71
D2N10	10	1.70 ± 0.10	13.59 ± 1.34	8.02 ± 0.57
D2N15	15	1.70 ± 0.10	15.54 ± 1.13	8.76 ± 0.42
D2N20	20	1.70 ± 0.10	17.06 ± 1.45	6.61 ± 0.49
D2N25	25	1.70 ± 0.10	13.70 ± 1.02	5.94 ± 0.36

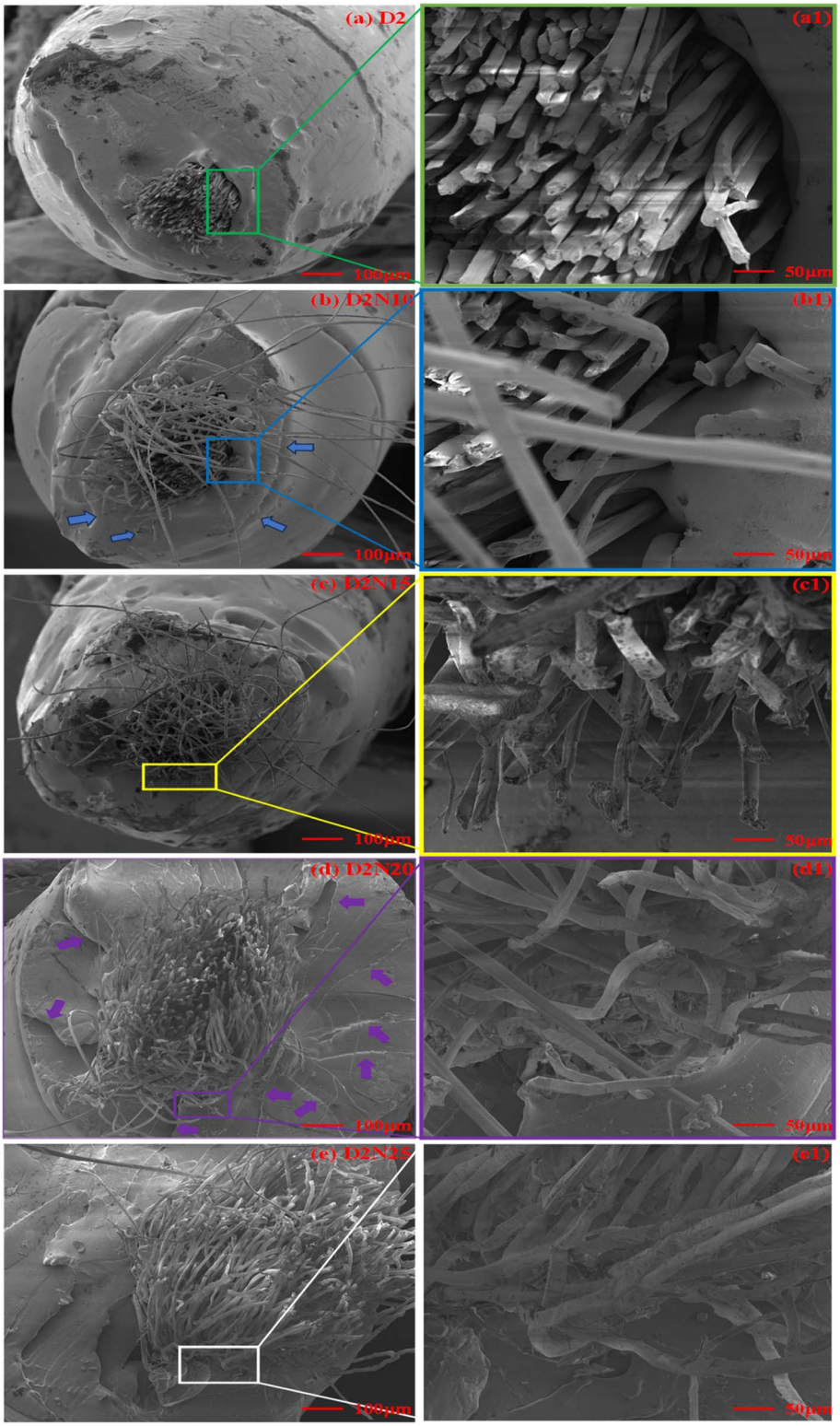

Fig. 8 Fractural morphologies affected by different alkali treatment times: (a) D2, (b) D2N10, (c) D2N15, (d) D2N20, and (e) D2N25. (a1), (b1), (c1), (d1) and (e1) is the enlargement of (a), (b), (c), (d) and (e), respectively.

3.4. Flexural properties of 3D-printed PCL/MS composites

Fig. 9 and Table 4 present the changes in flexural properties and morphology of PCL/MS composites prepared at various print temperatures, T90, T100, T110 and T120 represent the samples printed at 90 °C, 100 °C, 110 °C and 120 °C, respectively. All curves (Fig. 9i) climbed to the yield point after the elastic stage and gradually decreased as the flexural process continued, reaching almost 100% of tensile strain. To protect the testing

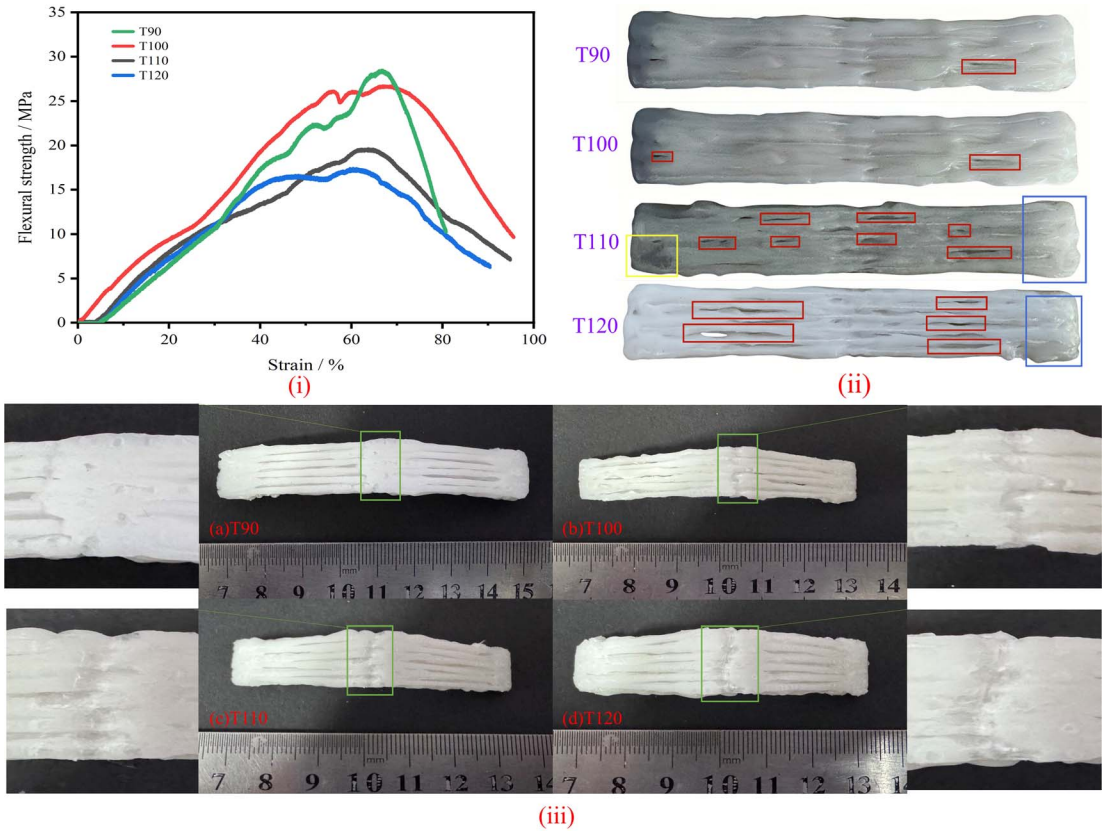

Fig. 9 Effect of print temperature on the flexural properties of 3D-printed PCL/MS composites: (i) strength–strain curves, (ii) specimens before being bended and (iii) specimens after being bended.

machine, the testing was manually stopped. The flexural strength of each group was obtained at the yield point. The T90 group exhibited the highest flexural strength (28.52 MPa) and the lowest porosity (15.29%), with almost no visible cracks after bending (Fig. 9iii, a). As the print temperature gradually increased, the flexural strength of the T100 group decreased slightly (26.07 MPa), and fewer cracks were observed in the printed specimen (Fig. 9iii, b), along with a noticeable increase in porosity (20.73%). Further increase in print temperature led to more pronounced declines in bending performance. T120 group displayed the lowest flexural strength (17.94 MPa), the highest porosity (35.33%) and the worst crack formation (Fig. 9iii, d).

As shown in Fig. 9ii, the printed specimens at higher temperatures exhibited an increase in void formation (red frame), along with material accumulation (blue frame) and material loss (yellow frame) at both ends of the specimen during printing. The crack patterns observed at maximum flexural deformation, illustrated in Fig. 9iii, reveal that higher print temperatures resulted in a greater number of cracks (green frame). This progressive increase in cracks directly resulted in the reduction of the flexural properties of the specimens. In addition, the actual size of the printed specimen and the original design size (80 mm × 10 mm × 4 mm) also showed a certain error. Higher temperatures resulted in a higher dimensional error. The length and width showed the maximum dimension deviation, with errors of 0.89 and 0.48 mm, respectively. In spite of the dimension deviation at the edge of specimens, the flexural testing was carried out smoothly with polishing treatment for specimens.

The reasons for the observed dimension deviation and increase in porosity can be attributed to the following factors: elevated temperatures reduced the viscosity of PCL, and increased the extrusion of PCL melts. The higher temperature might cause the thermal degradation of PCL,[53] which further resulted in the generation of pores between lines and layers. Incomplete cooling

Table 4 Flexural properties of 3D-printed PCL/MS composites

Specimen	Print temperature (°C)	Flexural strength (MPa)	Actual dimension (mm)	Porosity (%)
T90	90	28.52 ± 2.73	82.38 ± 0.89 × 11.45 ± 0.41 × 4.81 ± 0.42	7.40 ± 0.71
T100	100	26.07 ± 2.61	82.54 ± 0.49 × 11.51 ± 0.48 × 4.68 ± 0.10	8.02 ± 0.57
T110	110	19.61 ± 2.04	82.67 ± 0.12 × 11.75 ± 0.24 × 4.57 ± 0.02	8.76 ± 0.42
T120	120	17.94 ± 0.45	82.91 ± 0.19 × 12.19 ± 0.28 × 4.57 ± 0.21	6.61 ± 0.49

of the melts after extrusion resulted in material collapse or uneven deposition, which can subsequently give rise to dimensional inconsistencies and an augmentation in porosity.[54] Excessively high nozzle temperatures can result in a reduction in the surface quality and accuracy of the specimen.[55] Additionally, the route planning was not optimal; the amount of PLC melts at the lengthwise edge was more than in other sections, thus causing the excessive PLC accumulation at the edges.

3.5. Properties of porous scaffolds of PCL/MS composites

In the field of tissue engineering, the mechanical properties of bone are determined by its composition and structure. The porous scaffolds should be biocompatible, possess sufficient modulus, and provide an environment conducive to proliferation and differentiation of tissue cells.[50,56] Therefore, this study explored the properties of 3D printed porous scaffolds of PCL/MS composites.

Fig. 10 shows the PCL/MS composite porous scaffolds with various pore sizes. Table 5 illustrates the compression performance of these scaffolds as the pore size increased. P2, P2.5 and P3 represent samples with pore sizes of 2, 2.5 and 3 mm, respectively. The compressive strength decreased slightly from 10.75 MPa (P2) to 10.24 MPa (P3). Meanwhile, the compressive strain increased gradually with the increase in pore size. The P3 scaffold possessed the highest compressive strain (40.40%), exhibiting excellent deformability in compression. By contrast, the P2 scaffold exhibited the smallest compressive strain (31.97%), and the highest compression modulus (33.62 MPa), indicating its ability to resist deformation. In addition, all scaffolds demonstrated good shape retention post-compression, and maintained structural integrity under loading. Other studies obtained similar results. For example, PCL/HA scaffolds with larger pore sizes possessed lower compressive modulus and strength, but larger strain.[57]

The compressive modulus of human non-weight-bearing bone (10–2000 MPa)[58] provides critical benchmarking for biomaterial design. In comparison, the compressive strength of the PCL/MS composite scaffold in this study ranged from 25.33–33.62 MPa, indicating the scaffolds were suitable for use as non-weight-bearing bone substitutes.

3.6. Cytocompatibility evaluation of PCL/MS composites scaffold

Fig. 11 shows the results of cell viability and cytotoxicity tests. P0 represented the pure PCL porous scaffold, while P2 referred to the MS/PCL composite porous scaffold with a pore size of 2 mm. The results of the live/dead staining performed after 72 hours revealed that the majority of MC3T3-E1 cells in all groups remained viable, with only a small fraction of non-viable cells observed (as shown in Fig. 11i). These findings suggested that the materials under investigation did not exert a significant negative effect on cell survival during the incubation period. Furthermore, the CCK-8 assay provided additional confirmation of these observations. After 72 hours of incubation, the P2 scaffold did not exhibit any detrimental impact on the proliferation of MC3T3-E1 cells (as

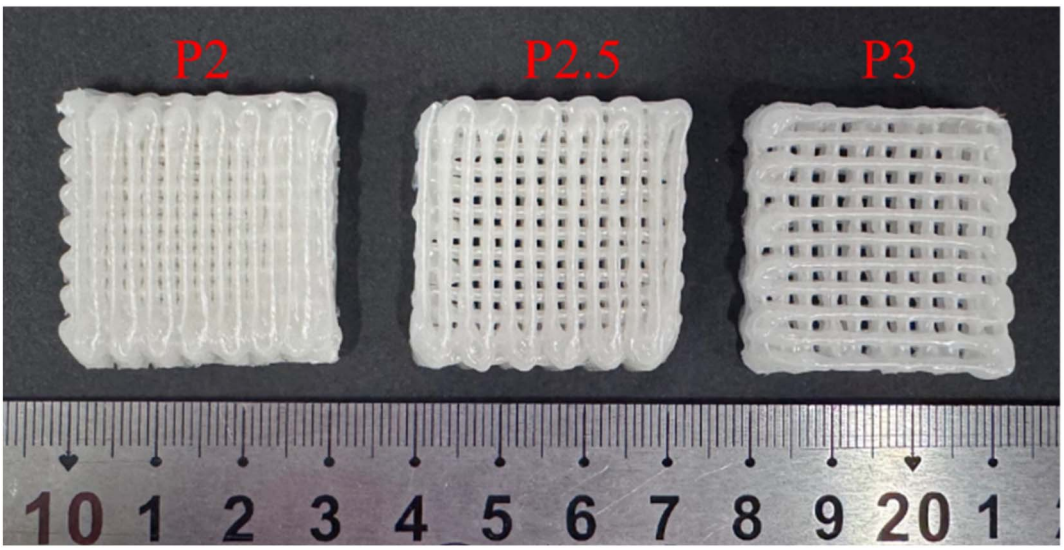

Fig. 10 Porous scaffolds of CL/MS composites.

Table 5 Compressive properties of specimens

Specimen	Pore size (mm)	Compression strength (MPa)	Compression strain (%)	Compression modulus (MPa)
P2	2.0 ± 0.14	10.75 ± 0.22	31.97 ± 2.15	33.62 ± 2.27
P2.5	2.5 ± 0.08	10.39 ± 0.16	38.84 ± 1.82	26.86 ± 1.93
P3	3.0 ± 0.07	10.24 ± 0.10	40.40 ± 1.76	25.33 ± 2.48

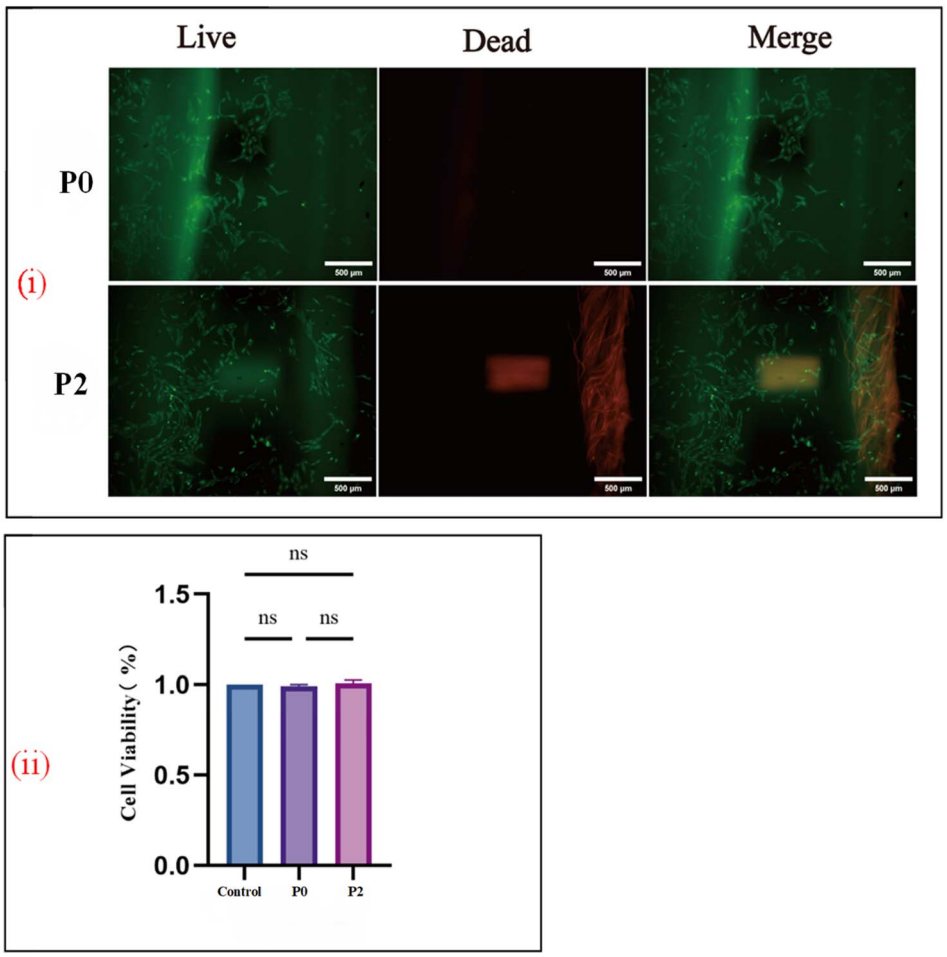

Fig. 11 (i) PCL/MS composite scaffold cell staining and (ii) toxicity test.

shown in Fig. 11ii). These results indicated that the fabricated composite scaffold demonstrated excellent biocompatibility, supporting both cell survival and proliferation, and making it a promising candidate for further bone tissue engineering applications.

4. Conclusion

This study utilized continuous mulberry silk to reinforce polycaprolactone (PCL) and investigated the properties of PCL/MS composite filaments and their 3D printed specimens. The MS fibers were subjected to alkali treatment for varying durations (10, 15, 20, and 25 minutes) to modify their surface properties. PCL/MS composite filaments, with and without alkali treatment, were prepared using a laboratory-scale single-screw extruder. The results showed that the incorporation of MS (ranging from 23.68% to 31.03% by weight) significantly improved the tensile strength of the PCL filaments from 9.52 to 21.02 MPa. Alkali treatment not only enhanced the tensile strength but also improved the interfacial compatibility between the PCL matrix and the MS continuous fibers.

The effect of print temperature on the flexural properties and dimensional accuracy of 3D printed PCL/MS composites was also examined. The results revealed that increasing the print temperature from 90 °C to 120 °C led to a decrease in flexural strength (from 28.52 to 17.94 MPa). Additionally, higher print temperatures resulted in greater dimensional inaccuracies. Therefore, it is crucial to control the print temperature around 90 °C to achieve optimal mechanical properties and dimensional precision.

Finally, PCL/MS composite porous scaffolds with pore sizes ranging from 2 to 3 mm were successfully fabricated. These scaffolds exhibited excellent compressive strength (10.24–10.75 MPa) and modulus (25.33–33.62 MPa), demonstrating their suitability for non-weight-bearing applications. Moreover, the porous scaffolds showed excellent biocompatibility in cell culture experiments, providing a non-toxic and favorable microenvironment for cell adhesion and proliferation. These findings highlighted the potential of PCL/MS composite scaffolds as promising candidates for use in tissue engineering and as implants for human bone repair.

Data availability

All data generated or analyzed during this study are included in the article.

Conflicts of interest

All authors declared that there are no conflicts of interest and no competing financial interests.

Acknowledgements

This paper was financially supported by the Institution of National Natural Science Foundations of China (52365043), Natural Science Foundations of Guangxi province (2023JJA160223, 2023JJA160056), Middle-aged and Young Teachers' Basic Ability Promotion Project of Guangxi (2020KY21012) and Guangxi Science and technology planning project (2023AB01248).

References

1 C. Accinelli, M. L. Sacca, M. Mencarelli, *et al.*, Deterioration of bioplastic carrier bags in the environment and assessment of a new recycling alternative, *Chemosphere*, 2012, **89**(2), 136–143.

2 A. Folino, A. Karageorgiou, P. S. Calabrò, *et al.*, Biodegradation of Wasted Bioplastics in Natural and Industrial Environments: A Review, *Sustainability*, 2020, **12**(15), 6030.

3 M. Mihai, N. Legros and A. Alemdar, Formulation-properties versatility of wood fiber biocomposites based on polylactide and polylactide/thermoplastic starch blends, *Polym. Eng. Sci.*, 2014, **54**(6), 1325–1340.

4 X. Wang, L. Huang, Y. Li, *et al.*, Research progress in polylactic acid processing for 3D printing, *J. Manuf. Process.*, 2024, **112**, 161–178.

5 S. K. Hedayati, A. H. Behravesh, S. Hasannia, *et al.*, 3D printed PCL scaffold reinforced with continuous biodegradable fiber yarn: a study on mechanical and cell viability properties, *Polym. Test.*, 2020, **83**, 106347.

6 J. John, N. Dyanti, T. Mokhena, *et al.*, Design and Development of Cellulosic Bionanocomposites from Forestry Waste Residues for 3D Printing Applications, *Materials*, 2021, **14**(13), 3462.

7 A. A. Vaidya, C. Collet, M. Gaugler, *et al.*, Integrating softwood biorefinery lignin into polyhydroxybutyrate composites and application in 3D printing, *Mater. Today Commun.*, 2019, **19**, 286–296.

8 S. A. Akbari Ghavimi, M. H. Ebrahimzadeh, M. Solati-Hashjin, *et al.*, Polycaprolactone/starch composite: fabrication, structure, properties, and applications, *J. Biomed. Mater. Res., Part A*, 2015, **103**(7), 2482–2498.

9 K. Li, J. Zhong, H. Guo, *et al.*, Preparation and Physicochemical Properties of PCL/HA Bone Tissue Engineer Porous Scaffold, *Polym. Bull.*, 2021, (05), 88–95.

10 C. Liu, Y. Chen, J. Wang, *et al.*, Research Progress on Properties and Applications of Biodegradable Materials, *Plast. Sci. Technol.*, 2022, **50**(07), 81–85.

11 M. Thakur, I. Majid, S. Hussain, *et al.*, Poly(ε-caprolactone): a potential polymer for biodegradable food packaging applications, *Packag. Technol. Sci.*, 2021, **34**(8), 449–461.

12 E. Drago, R. Campardelli, I. D. Marco, *et al.*, Optimization of PCL Polymeric Films as Potential Matrices for the Loading of Alpha-Tocopherol by a Combination of Innovative Green Processes, *Processes*, 2021, **9**(12), 2244.

13 J. Bai, *Preparation and Properties of Degradable Materials and Sensing Materials Based on Natural Fiber*, Wuhan Textile University, 2023.

14 J. Yao, *Research on the Poly (Lactic Acid) Biodegradable Composites Reinforced with Plant Fibers and Their Derivatives*, Hunan University of Technology, 2018.

15 M. A. Mahmud, N. Abir, F. R. Anannya, *et al.*, Coir fiber as thermal insulator and its performance as reinforcing material in biocomposite production, *Heliyon*, 2023, **9**(5), e15597.

16 N. Karthi, K. Kumaresan, S. Sathish, *et al.*, An overview: natural fiber reinforced hybrid composites, chemical treatments and application areas, *Mater. Today: Proc.*, 2020, **27**, 2828–2834.

17 T. Hassan, H. Jamshaid, R. Mishra, *et al.*, Acoustic, Mechanical and Thermal Properties of Green Composites Reinforced with Natural Fibers Waste, *Polymers*, 2020, **12**(3), 654.

18 F. Sarasini, J. Tirillò, D. Puglia, *et al.*, Biodegradable polycaprolactone-based composites reinforced with ramie and borassus fibres, *Compos. Struct.*, 2017, **167**, 20–29.

19 H. N. Dhakal, S. O. Ismail, J. Beaugrand, *et al.*, Characterization of Nano-Mechanical, Surface and Thermal Properties of Hemp Fiber-Reinforced Polycaprolactone (HF/PCL) Biocomposites, *Appl. Sci.*, 2020, **10**(7), 2636.

20 R. Malinowski, A. Raszkowska-Kaczor, K. Moraczewski, *et al.*, The Structure and Mechanical Properties of Hemp Fibers-Reinforced Poly(ε-Caprolactone) Composites Modified by Electron Beam Irradiation, *Appl. Sci.*, 2021, **11**(12), 5317.

21 G. S. Perrone, G. G. Leisk, T. J. Lo, *et al.*, The use of silk-based devices for fracture fixation, *Nat. Commun.*, 2014, **5**, 3385.

22 K. Lerdchai, J. Kitsongsermthon, J. Ratanavaraporn, *et al.*, Thai Silk Fibroin/Gelatin Sponges for the Dual Controlled Release of Curcumin and Docosahexaenoic Acid for Anticancer Treatment, *J. Pharm. Sci.*, 2016, **105**(1), 221–230.

23 Z. X. Cai, X. M. Mo, K. H. Zhang, *et al.*, Fabrication of chitosan/silk fibroin composite nanofibers for wound-dressing applications, *Int. J. Mol. Sci.*, 2010, **11**(9), 3529–3539.

24 N. Minoura, S. I. Aiba, M. Higuchi, *et al.*, Attachment and Growth of Fibroblast Cells on Silk Fibroin, *Biochem. Biophys. Res. Commun.*, 1995, **208**(2), 511–516.

25 G. Guan, L. Wang, M. Li, *et al.*, In vivo biodegradation of porous silk fibroin films implanted beneath the skin and muscle of the rat, *Bio-Med. Mater. Eng.*, 2014, **24**, 789–797.

26 Y. Ma, Z. Li, R. Ran, *et al.*, Research on Application of Silk in Biomaterial Field, *Mater. Rep.*, 2018, **32**(01), 86–92.

27 J. Zhang, Q. Jia, E. Meng, *et al.*, Characteristics of electrospun membranes in different spidroin/PCL ratios, *Biomed. Mater.*, 2021, **16**(6), 065022.

28 T. Li, *Study on Preration and Mechanical Properties of Silk/PLA and PCL Composites*, Zhejiang Sci-Tech University, 2019.

29 R. Shi, D. Ye, K. Ma, *et al.*, Understanding the Interfacial Adhesion between Natural Silk and Polycaprolactone for

Fabrication of Continuous Silk Biocomposites, *ACS Appl. Mater. Interfaces*, 2022, **14**(41), 46932–46944.

30 X. Bi, X. Tian, S. Zhang, *et al.*, Research Progress in 3D Printing Technology of Continuous Fiber Reinforced Thermoplastic Composites, *Eng. Plast. Appl.*, 2019, **47**(02), 138–142.

31 P. Parandoush and D. Lin, A review on additive manufacturing of polymer-fiber composites, *Compos. Struct.*, 2017, **182**, 36–53.

32 A. G. Scott, S. Robert and N. T. Brian, A review of melt extrusion additive manufacturing processes: I. Process design and modeling, *Rapid Prototyp. J.*, 2014, **20**(3), 192–204.

33 P. Bettini, G. Alitta, G. Sala, *et al.*, Fused Deposition Technique for Continuous Fiber Reinforced Thermoplastic, *J. Mater. Eng. Perform.*, 2016, **26**(2), 843–848.

34 Y. Zhao, J. Yang, X. Ding, *et al.*, Polycaprolactone/polysaccharide functional composites for low-temperature fused deposition modelling, *Bioact. Mater.*, 2020, **5**(2), 185–191.

35 Y. Wang, J. Zhang, M. Li, *et al.*, 3D printing thermo-responsive shape memory polymer composite based on PCL/TPU blends, *J. Polym. Res.*, 2022, **29**(6), 243.

36 Y. Wang, Y. Wang, Q. Wei, *et al.*, Effects of the composition ratio on the properties of PCL/PLA blends: a kind of thermo-sensitive shape memory polymer composites, *J. Polym. Res.*, 2021, **28**(12), 451.

37 N. Li, Y. Li and S. Liu, Rapid prototyping of continuous carbon fiber reinforced polylactic acid composites by 3D printing, *J. Mater. Process. Technol.*, 2016, **238**, 218–225.

38 T. A. Augusto, M. C. Crovace and L. C. Costa, Continuous glass fiber-reinforced polycaprolactone composite produced in a conventional fused filament fabrication equipment: process modeling and parameters adjustment, *J. Appl. Polym. Sci.*, 2024, **141**(42), e56090.

39 J. Cheng, Y. Wang, L. Xing, *et al.*, Research on the surface treatment and electrical conductivity of silk fibers, *Jiangsu Silk*, 2022, (06), 27–32.

40 M. Latos-Brozio and A. Masek, Effect of Impregnation of Biodegradable Polyesters with Polyphenols from *Cistus linnaeus* and *Juglans regia* Linnaeus Walnut Green Husk, *Polymers*, 2019, **11**(4), 669.

41 A. I. Susanin, E. S. Sashina, V. V. Zakharov, *et al.*, Structural Changes of Fibroin During Chemical Processing of Silk Wastes, *Fibre Chem.*, 2020, **51**(6), 412–417.

42 M. A. Koperska, J. Bagniuk, M. M. Zaitz-Olsza, *et al.*, *Ex Situ* and *In Situ* Artificial Thermo-Aging Study of the Natural Degradation of *Bombyx mori* Silk Fibroin, *Appl. Sci.*, 2023, **13**(16), 9427.

43 X. Luo, Y. Du, M. Shen, *et al.*, investigation of Fibrous Cultural Materials by Infrared Spectroscopy, *Spectrosc. Spectral Anal.*, 2015, **35**(01), 60–64.

44 J. Zhong, X. Zhou and C. Ye, *et al.*, Using FTIR Imaging to Investigate Silk Fibroin-Based Materials [M]//LING, *Fibrous Proteins: Design, Synthesis, and Assembly*, New York, NY, Springer US, 2021, pp. 207–219.

45 R. Arunkumar, C. J. Drummond and T. L. Greaves, FTIR Spectroscopic Study of the Secondary Structure of Globular Proteins in Aqueous Protic Ionic Liquids, *Front. Chem.*, 2019, **7**, 74.

46 A. Tong, Z. Shi, S. Qiao, *et al.*, Research progress in high-performance/multifunctional silk fibers, *Basic Sci. J. Text. Univ.*, 2024, **37**(02), 1–13.

47 N. Kasoju and U. Bora, Silk fibroin in tissue engineering, *Adv. Healthcare Mater.*, 2012, **1**(4), 393–412.

48 Y. Yin and J. Xiong, Effect of the Distribution of Fiber Orientation on the Mechanical Properties of Silk Fibroin/Polycaprolactone Nanofiber Mats, *J. Eng. Fibers Fabr.*, 2017, **12**(3), 155892501701200303.

49 R. Shi, T. W. Dongdo, *et al.*, Understanding the Interfacial Adhesion between Natural Silk and Polycaprolactone for Fabrication of Continuous Silk Biocomposites, *ACS Appl. Mater. Interfaces*, 2022, **14**(41), 46932–46944.

50 S. Sheik, G. K. Nagaraja, J. Naik, *et al.*, Development and characterization study of silk fibre reinforced poly(vinyl alcohol) composites, *Int. J. Plast. Technol.*, 2017, **21**(1), 108–122.

51 M. T. Zafar, S. N. Maiti and A. K. Ghosh, Effect of surface treatment of jute fibers on the interfacial adhesion in poly(lactic acid)/jute fiber biocomposites, *Fibers Polym.*, 2016, **17**(2), 266–274.

52 G. Li, H. Liu, T. Li, *et al.*, Surface modification and functionalization of silk fibroin fibers/fabric toward high performance applications, *Mater. Sci. Eng., C*, 2012, **32**(4), 627–636.

53 F. Rivera-Lopez, M. M. L. Pavon, E. C. Correa, *et al.*, Effects of Nozzle Temperature on Mechanical Properties of Polylactic Acid Specimens Fabricated by Fused Deposition Modeling, *Polymers*, 2024, **16**(13), 1867.

54 G. D. Goh, Y. L. Yap, H. K. J. Tan, *et al.*, Process–Structure–Properties in Polymer Additive Manufacturing *via* Material Extrusion: A Review, *Crit. Rev. Solid State Mater. Sci.*, 2019, **45**(2), 113–133.

55 F. de Freitas and H. Pegado, Impact of nozzle temperature on dimensional and mechanical characteristics of low-density PLA, *Int. J. Adv. Des. Manuf. Technol.*, 2023, **126**(3–4), 1629–1638.

56 X. Liu and P. X. Ma, Polymeric Scaffolds for Bone Tissue Engineering, *Ann. Biomed. Eng.*, 2004, **32**(3), 477–486.

57 N. Rezania, M. Asadi-Eydivand, N. Abolfathi, *et al.*, Three-dimensional printing of polycaprolactone/hydroxyapatite bone tissue engineering scaffolds mechanical properties and biological behavior, *J. Mater. Sci.:Mater. Med.*, 2022, **33**(3), 31.

58 X. Song, W. He, S. Yang, *et al.*, Fused Deposition Modeling of Poly(Lactic Acid)/Walnut Shell Biocomposite Filaments—Surface Treatment and Properties, *Appl. Sci.*, 2019, **9**(22), 4892.